Monthly Notices of the ROYAL ASTRONOMICAL SOCIETY

MNRAS **453,** 229–241 (2015) doi:10.1093/mnras/stv1571

Updated analytical solutions of continuity equation for electron beams precipitation – I. Pure collisional and pure ohmic energy losses

R. R. Dobranskis★ and V. V. Zharkova

Department of Mathematics and Information Sciences, University of Northumbria, Newcastle upon Tyne, NE1 2XP, UK

Accepted 2015 July 10. Received 2015 July 10; in original form 2015 May 23

ABSTRACT

We present updated analytical solutions of continuity equations for power-law beam electrons precipitating in (a) purely collisional losses and (b) purely ohmic losses. The solutions of continuity equation (CE) normalized on electron density presented in Dobranskis & Zharkova are found by method of characteristics eliminating a mistake in the density characteristic pointed out by Emslie et al. The corrected electron beam differential densities (DD) for collisions are shown to have energy spectra with the index of $-(\gamma + 1)/2$, coinciding with the one derived from the inverse problem solution by Brown, while being lower by $1/2$ than the index of $-\gamma/2$ obtained from CE for electron flux. This leads to a decrease of the index of mean electron spectra from $-(\gamma - 2.5)$ (CE for flux) to $-(\gamma - 2.0)$ (CE for electron density). The similar method is applied to CE for electrons precipitating in electric field induced by the beam itself. For the first time, the electron energy spectra are calculated for both constant and variable electric fields by using CE for electron density. We derive electron DD for precipitating electrons (moving towards the photosphere, $\mu = +1$) and 'returning' electrons (moving towards the corona, $\mu = -1$). The indices of DD energy spectra are reduced from $-\gamma - 1$ (CE for flux) to $-\gamma$ (CE for electron density). While the index of mean electron spectra is increased by 0.5, from $-\gamma + 0.5$ (CE for flux) to $-\gamma + 1$(CE for electron density). Hard X-ray intensities are also calculated for relativistic cross-section for the updated differential spectra revealing closer resemblance to numerical Fokker–Planck (FP) solutions.

Key words: plasmas – Sun: atmosphere – Sun: flares – Sun: particle emission – Sun: X-rays, gamma rays.

1 INTRODUCTION

The first interpretation of the power-law energy spectra observed in hard X-ray (HXR) emission from solar flares was derived from the inverse problem solution (Brown 1971) that formed the foundation of high-energy physics in the Sun. Later the analytical solutions for electron precipitation in flaring atmosphere described by continuity equation (CE) for electron flux were also derived (Syrovatskii & Shmeleva 1972) providing an effective way for observers to link the measured HXR photon counts and their power-law energy spectra to the distributions of precipitating electrons scattered on the ambient plasma particles. Both approaches agreed on the power-law energy spectra of precipitating electron flux with a spectral index $-\gamma$ leading to mean electron spectra (MES) having the spectral indices of $-(\gamma - 2.0)$. A number of authors calculated HXR emission from Fokker–Planck (FP) simulations considering collisional losses and magnetic mirroring effect also using relativistic bremsstrahlung cross-sections of bremsstrahlung emission produced by beam electrons (see for example Bai & Ramaty 1978; Leach & Petrosian 1981) that in some events could account better for the observational features that the analytical approach.

Although, purely collisional approach highlighted the problem of a large number of beam electrons (10^{36}–10^{37} particles s^{-1}) required to produce the observed HXR photons from a single flare (Brown 1972). These numbers would imply that any acceleration mechanism producing these electrons in flares needs to energize to high sub-relativistic energies the whole population of the ambient electrons at the coronal level, which is rather difficult to achieve. This introduced the so-called particle number problem (Brown 1972), which puzzled researchers for a few decades.

Later it was established that electron beams precipitating into flaring atmosphere induce an electrostatic electric field, which slows down precipitating electrons and produces a return current leading to substantial ohmic losses (Knight & Sturrock 1977; Emslie 1980; Diakonov & Somov 1988; Haydock et al. 2001). This allowed us to extend interpretation of the observed HXR emission produced by precipitating electron beams from the approach considering only purely Coulomb collisions (Brown 1971; Syrovatskii & Shmeleva 1972) to consideration of ohmic losses of electrons in the

★ E-mail: rytis.dobranskis@northumbria.ac.uk

electrostatic electric field (Emslie 1980; McClements 1992) by considering a return current formed by the ambient electrons only, as suggested by Knight & Sturrock (1977).

Further progress with high-resolution observations, made by the *RHESSI* payload, have provided a significant amount of accurate data that allowed the scientists to understand better the evolution of photon and electron spectra during solar flares and to provide locations and shapes of the HXR sources on the solar disc (Holman et al. 2003, 2011; Lin et al. 2003; Brown et al. 2006; Krucker et al. 2008). It was revealed that many powerful flares produce the elbow-type HXR photon spectra with double power-law energy distributions (Kontar, Brown & McArthur 2002; Conway et al. 2003; Holman et al. 2003). The investigation of various aspects of the photospheric albedo effects has shown that reflection of HXR emission from the photosphere can be important in the interpretation of HXR energy spectra (Brown et al. 2006; Kontar & Brown 2006).

Moreover, MES, obtained by the inversion of photon spectra measured from the *RHESSI* payload (Piana et al. 2003) revealed noticeable dips at lower energies between 20 and 40 keV with the maximum occurring at higher energies (50–80 keV). The dips occur at the same energies where the corresponding HXR photon spectra have noticeable flattening towards lower energies. Initially, the flattening of HXR photon spectra was attempted to be explained by purely collisional model with an increased lower cut-off energy by shifting it to the turning point where HXR emission flattens (Sui, Holman & Dennis 2005). However, in some case the lower cut-off energy should be shifted to 60–80 keV that raises some doubts about this interpretation.

These new puzzles required to extend the interpretation of observed HXR emission produced by precipitating electron beams from the purely collisional approach to consideration of ohmic losses by beam electrons in a self-induced electrostatic electric field (Diakonov & Somov 1988; Zharkova, Brown & Syniavskii 1995; Zharkova & Gordovskyy 2005, 2006; Sui, Holman & Dennis 2007). Since the energy losses in electric field are found to substantially decrease a precipitation depth of energetic electrons (Zharkova & Gordovskyy 2006), then the number of low-energy (<100 keV) precipitating electrons is also substantially decreased, when ohmic losses are considered in addition to collisions.

This can lead to electron beams with greater initial energy flux to induce a stronger electric field and, thus, to have higher ohmic losses, which lead to a greater flattening of their photon spectra at lower energies (Zharkova & Gordovskyy 2006; Sui et al. 2007). Also, ohmic losses of beam electrons (Zharkova & Gordovskyy 2006) combined with the HXR albedo effect at its reflection from the photosphere (Massone et al. 2004) can be successfully deployed for the explanation of a full drop of MES in the dips reported by Piana et al. (2003).

However, full understanding of the role of a self-induced electric field on electron beam dynamics came only from the simulation in the Fokker–Planck approach of the time-dependent injection of power-law electrons (Siversky & Zharkova 2009). The authors derived for the first time from the Fokker–Planck simulations that during a steady injection of power-law electrons into a flaring atmosphere the main part of returning electrons is formed from the precipitating electrons scattered to pitch angles with negative pitch angle cosines (or returning beam electrons). This approach is essentially different from the earlier one (Knight & Sturrock 1977) considering a return current formed by the ambient electrons.

In the other words, precipitating and returning beam electrons form an electric circuit from the corona to the photosphere where beam electrons are recycled, or, while the injection exists, they travel many times up and down (Siversky & Zharkova 2009). The characteristic time-scale for creation of this electric circuit ranges from 0.07 to 0.1 s, while the travel time of relativistic beam electrons from the corona to the photosphere is about 0.01–0.1 s. This means that after the first 0.07–0.1 s when the circuit is established the beam electrons can make up to 10–100 journeys downwards and upwards. This resolves the particle number problem because in this case only (1–10) per cent of the ambient electrons is required to account for the observed HXR photon numbers.

Therefore, the aim of this paper is to continue the research presented in Dobranskis & Zharkova (2014) by correcting the analytical solution found from CE for the electron density following the correction proposed by Emslie, Holman & Litvinenko (2014) and finding in the same approach the analytical solutions of CE for electron precipitation in ohmic losses. We will explore separate effects of energy loss mechanisms on resulting electron energy spectra, mean electrons spectra and their HXR emission that allows us to derive a future possibility to find joint analytical solutions for a quick fit of observational data to model calculations with mixed energy losses that is a scope of the forthcoming Paper II.

2 THE CORRECTED SOLUTIONS FOR COLLISIONAL LOSSES

2.1 The original CE for electron flux

The flux of precipitating electron beams $F = v \times N$ can be derived from a CE for an electron beam flux (Syrovatskii & Shmeleva 1972)

$$\frac{\partial}{\partial s}[vN(E,s)] + \frac{\partial}{\partial E}\left[\left(\frac{\mathrm{d}E}{\mathrm{d}s}\right) vN(E,s)\right] = 0, \tag{1}$$

where v is the beam electron velocity and N defines the density of the beam electrons with the velocity v, while the term $\frac{\mathrm{d}E}{\mathrm{d}s}$ defines the energy losses. To simplify equation (1) Syrovatskii & Shmeleva (1972) introduce a new function

$$\varphi(E,\xi) = \frac{1}{n(s)}\left(\frac{\mathrm{d}E}{\mathrm{d}s}\right) vN(E,s) = \left(\frac{\mathrm{d}E}{\mathrm{d}\xi}\right) vN(E,\xi), \tag{2}$$

where n defines ambient plasma density and ξ is a column depth:

$$\xi(s) = \int_0^s n(t)\,\mathrm{d}t, \tag{3}$$

which defines a total number of particles in the line of sight within an area of one square centimetre.

Equation (2) is used to rewrite the CE (1) in the following way:

$$\frac{\partial}{\partial s}\left[\frac{n(s)\varphi(E,\xi)}{\mathrm{d}E/\mathrm{d}s}\right] + \frac{\partial}{\partial E}[n(s)\varphi(E,\xi)] = 0. \tag{4}$$

Then substituting the expression for collisional energy losses

$$\frac{\mathrm{d}E}{\mathrm{d}s} = -\frac{an}{E} \tag{5}$$

into equation (4) and multiplying the result by $-\frac{a}{En}$ produces the first-order partial differential equation (PDE) for the function φ:

$$\frac{\partial}{\partial \xi}\varphi(E,\xi) - \frac{a}{E}\frac{\partial}{\partial E}\varphi(E,\xi) = 0. \tag{6}$$

The CE is a PDE with two independent variables: a linear electron precipitation depth s (cm) and an electron kinetic energy E (eV), which is solved using the method of characteristics (Courant & Hilbert 1962), producing characteristic equations $\xi = t$, $E_0 = \sqrt{E^2 + 2a\xi}$ and general solution for the function φ:

$$\varphi(E,\xi) = \Psi(\sqrt{E^2 + 2a\xi}), \tag{7}$$

where Ψ is an arbitrary function. Then the general solution for electron differential density N is obtained by inverting equation (2) and substituting it with general solution for φ (equation 7), expression for collisional energy losses (equation 5), and $v = \sqrt{2E/m}$ (where $\sqrt{2/m}$ is recalled in normalization constant):

$$\begin{aligned} N &= \frac{\varphi}{(\mathrm{d}E/\mathrm{d}s)\, v} = \frac{\Psi(\sqrt{E^2+2a\xi})}{|-a/E_0|\sqrt{E_0}} \\ &= \Psi(\sqrt{E^2+2a\xi}) \times \sqrt{E_0} \\ &= \Psi(\sqrt{E^2+2a\xi}) \times \left(E^2+2a\xi\right)^{1/4}. \end{aligned} \tag{8}$$

To obtain the final (original) solution of PDE, let us use the boundary condition, which defines the initial power-law energy spectrum of electrons at the upper boundary, where $\xi = 0$ cm^{-2} (Syrovatskii & Shmeleva 1972):

$$\begin{aligned} N(E,0) = K E^{-\left(\gamma+\frac{1}{2}\right)} \\ \times \Theta\,(E - E_{\mathrm{low}})\,\Theta\,(E_{\mathrm{upp}} - E), \end{aligned} \tag{9}$$

where γ is a spectral index of the electron flux $F = vN(E, s)$. Hence, in order to keep the spectral index for flux equal to γ, the initial electron density has to be reduced by $E^{-1/2}$); E_{low} and E_{upp} are the lower and upper energy cut-offs, respectively; Θ is the Heavyside step function and K is the scaling factor, found from normalization of the distribution function on electron flux (for CE for flux, equation 1) or on electron density (for CE for density, see Section 2.2).

The solution of CE (6) after a substitution of initial condition (9) above yields the following form of differential density for precipitating beam electrons:

$$\begin{aligned} N(E,\xi) = K \left(E^2+2a\xi\right)^{-\gamma/2} \\ \times \Theta\left(\sqrt{E^2+2a\xi} - E_{\mathrm{low}}\right) \\ \times \Theta\left(E_{\mathrm{upp}} - \sqrt{E^2+2a\xi}\right). \end{aligned} \tag{10}$$

Where spectral index is obtained as $-\frac{\gamma}{2} = -\frac{\gamma+0.5}{2} + \frac{1}{4}$, and the constant of integration K is defined from the initial energy flux $F_0 = vN(E, 0)$ of beam electrons at the top boundary ($\xi = 0$) as follows (Syrovatskii & Shmeleva 1972):

$$\begin{aligned} F_0 &= \int_{E_{\mathrm{low}}}^{E_{\mathrm{upp}}} E v N(E,0)\,\mathrm{d}E \\ &= K\left(\frac{2}{m}\right)^{1/2} \int_{E_{\mathrm{low}}}^{E_{\mathrm{upp}}} E^{1-\gamma}\mathrm{d}E \\ &= K\left(\frac{2}{m}\right)^{1/2} \begin{cases} \frac{E_{\mathrm{upp}}^{\gamma-2} - E_{\mathrm{low}}^{\gamma-2}}{2-\gamma}, & \gamma \neq 2, \\ ln\left(\frac{E_{\mathrm{upp}}}{E_{\mathrm{low}}}\right), & \gamma = 2. \end{cases} \end{aligned} \tag{11}$$

Then the scaling factor K is calculated from equation (11) with the initial energy flux, spectral index and cut-off energies to be considered as free parameters set up by a modeller or derived from the observation (Syrovatskii & Shmeleva 1972).

The solution (10), found from CE for electron flux presented in the paper by Syrovatskii & Shmeleva (1972, equation 1 and 6), has a different spectral index for the energy spectra with the argument $E^2 + 2a\xi$. In fact, the index in solution (10) is lower by 1/2 than one reported by Syrovatskii & Shmeleva (1972, their equation 9) and from index derived by Brown (1971) from the inverse problem solution. The reason for this difference is discussed in the section below.

2.2 The updated CE approach for electron density

2.2.1 General modification of CE

In order to obtain the accurate solutions normalized on the electron density of precipitating electrons, one needs to obtain CE for the electron density N, and not for its flux F (Dobranskis & Zharkova 2014). In order to obtain this equation, let us substitute into original CE (1) a classic link between velocity v and energy E, $v = \sqrt{2E/m}$. Then the updated CE can be written in the following form:

$$\frac{\partial}{\partial s}\left[\sqrt{\frac{2E}{m_e}}N(E,s)\right] + \frac{\partial}{\partial E}\left[\left(\frac{\mathrm{d}E}{\mathrm{d}s}\right)\sqrt{\frac{2E}{m_e}}N(E,s)\right] = 0. \tag{12}$$

This equation can be transformed (similar to Dobranskis & Zharkova 2014) to

$$\begin{aligned} \sqrt{E}\frac{\partial N}{\partial s} + \left[\frac{\partial}{\partial E}\left(\frac{\partial E}{\partial s}\right)\sqrt{E}N\right] \\ + \left(\frac{\partial E}{\partial s}\right)\left(\sqrt{E}\frac{\partial N}{\partial E} + \frac{1}{2}E^{-1/2}N\right) = 0. \end{aligned} \tag{13}$$

2.2.2 The corrected solutions of CE for electron density

The corrected first-order PDE for density N, derived by Dobranskis & Zharkova (2014, their equation 13), can be obtained from equation (13) by substituting into it energy loss equation (5):

$$\frac{\partial N}{\partial \xi} - \frac{a}{E}\frac{\partial N}{\partial E} = -\frac{aN}{2E^2}. \tag{14}$$

It is assumed that the values of all variables ξ, E and N are known on some initial curve (the boundary condition):

$$\xi(0) = \xi_0, \qquad E(0) = E_0, \qquad N(0) = N_0, \tag{15}$$

where E and N are given as a functions of ξ. Then the original CE equation can be replaced with its characteristics (Courant & Hilbert 1962) for each variable: ξ, E and N.

Let us now correct the solution of CE for the electron density derived in Dobranskis & Zharkova (2014, or normalized on electron density, similar to Diakonov & Somov 1988) following the correction proposed by Emslie et al. (2014). The solution of CE for the electron density presented by Dobranskis & Zharkova (2014) had a mistake pointed out by Emslie et al. (2014), which occurred during the application of the method of characteristics for differential density N.

The characteristic equations are solved as follows:

$$\frac{\mathrm{d}\xi}{\mathrm{d}t} = 1 \;\rightarrow\; \xi(0) = 0 \;\rightarrow\; \xi = t\ldots(+\xi_0), \tag{16}$$

$$\begin{aligned} \frac{\mathrm{d}E}{\mathrm{d}t} = -\frac{a}{E} \;\rightarrow\; E(0) = E_0 \\ \rightarrow\; \frac{E^2}{2} = -at + \frac{E_0^2}{2} \rightarrow\; E_0 = \sqrt{E^2+2a\xi}, \end{aligned} \tag{17}$$

$$\frac{\mathrm{d}N}{N} = -\frac{1}{2}\frac{a}{E^2}\mathrm{d}t \;\rightarrow\; \frac{\mathrm{d}N}{N} = -\frac{1}{2}\frac{a}{E_0^2 - 2at}\mathrm{d}t. \tag{18}$$

In the last characteristic equation (18), we used the correction proposed by Emslie et al. (2014), e.g. the energy E is substituted

with the expression $E^2 = E_0^2 - 2at$ obtained from the characteristic equation (17) for E.

The characteristic equation for N (18) can then be integrated, to produce solution:

$$\ln(N)_{N_0}^{N} = \frac{1}{4}\ln(u)|_{u_0}^{u}$$
$$\rightarrow \quad N = N_0 \times (u)^{1/4} \times (u_0)^{-1/4}. \tag{19}$$

Then, after making relevant substitutions:

$$u(t) = E_0^2 - 2at,$$
$$u_0(t=0) = E_0^2. \tag{20}$$

By substituting the expressions (20) for $u(t)$ and $u_0(t)$ into the solution (19) one can easily obtain the general solution in the following form:

$$N(E,\xi) = \Psi(\sqrt{E^2+2a\xi}) \times E^{1/2} \times \left(E^2+2a\xi\right)^{-1/4}. \tag{21}$$

Equation (21) still has an additional factor of $(E^2+2a\xi)^{-1/4}$ (the last term in equation 21) appearing in the CE for N. While the solution (equation 10) of CE for electron flux Nv has the two different factors: $\Psi(\sqrt{E^2+2a\xi}) \times (E^2+2a\xi)^{1/4}$.

Verification of the solution: an alternative method (Ruderman, private communication) can be used to verify the general solution of CE for purely collisional losses (21) as follows.

The characteristics of equation (14) are defined by energy loss equation (5), which has a solution in form of $E^2 + 2a\xi =$ constant. As a result, a new variable $\eta = \sqrt{E^2+2a\xi}$ is introduced instead of column depth ξ.

Then using the relations:

$$\frac{\partial N}{\partial \xi} = \frac{a}{\eta}\frac{\partial N}{\partial \eta}, \quad \left.\frac{\partial N}{\partial E}\right|_{\xi} = \left.\frac{\partial N}{\partial E}\right|_{\eta} + \frac{\partial N}{\partial \eta}\frac{\partial \eta}{\partial E} = \left.\frac{\partial N}{\partial E}\right|_{\eta} + \frac{E}{\eta}\frac{\partial N}{\partial \eta}, \tag{22}$$

where the subscripts ξ and η indicate that the derivative is calculated at constant ξ and constant η, respectively, then equation (14) is effectively reduced to

$$\left.\frac{\mathrm{d}N}{\mathrm{d}E}\right|_{\eta} = \frac{N}{2E}. \tag{23}$$

The general solution to equation (23) is $N = E^{1/2}F(\eta)$, where F is an arbitrary functions. Introducing function $\Psi(\eta) = \eta^{1/2}F(\eta)$, and rescaling the definition of η, we eventually arrive at

$$N(E,\xi) = \Psi(\sqrt{E^2+2a\xi}) \times E^{1/2} \times \left(E^2+2a\xi\right)^{-1/4}, \tag{24}$$

which is essentially the same general CE solution (21), presented above.

Final solution for differential densities: finally, substitution of the initial condition (equation 9) into the solution (21) produces the corrected solution of CE for N:

$$N(E,\xi) = KE^{1/2}\left(E^2+2a\xi\right)^{-\frac{\gamma+0.5}{2}-\frac{1}{4}} \times \Theta\left(\sqrt{E^2+2a\xi} - E_{\rm low}\right) \times \Theta\left(E_{\rm upp} - \sqrt{E^2+2a\xi}\right)$$
$$= KE^{1/2}\left(E^2+2a\xi\right)^{-\frac{\gamma+1}{2}} \times \Theta\left(\sqrt{E^2+2a\xi} - E_{\rm low}\right) \times \Theta\left(E_{\rm upp} - \sqrt{E^2+2a\xi}\right). \tag{25}$$

Here, the scaling factor K is estimated through normalization of this function on a beam density N_0 at the top boundary by equating it to the ambient plasma density or its fraction (see Section 3.1).

In fact, the corrected solution (25) for differential density N is exactly the solution reported by (Syrovatskii & Shmeleva 1972) and Brown (1971), with the power index of the term $E^2 + 2a\xi$ being equal to $-\frac{\gamma+1}{2}$ and not to $-\frac{\gamma}{2}$ as appears from the CE for electron flux Nv (see equation 10). The solution for flux does not contain the $\sqrt{E}$ term, which is present in corrected solution for density.

Of course, this corrected solution still has an additional exponential term of the argument $E^2 + 2a\xi$ with a power of $-1/4$, as indicated by Emslie et al. (2014) and not the exponent of the ratio between E and $2a\xi$, mistakenly reported by Dobranskis & Zharkova (2014). This exponential correction still means that, in order to obtain the index reported in the paper by Syrovatskii & Shmeleva (1972) one has to solve the equation for the electron density (equation 14) and not the CE for electron flux (equation 6) claimed in the paper.

To stay in line with the proposed correction, the scaling factor K, estimated through normalization on electron flux, must be normalized on an electron beam density at the top boundary ($\xi = 0$). The normalization is done by integration of the boundary condition for energy E (equation 9) as follows:

$$N_0(\xi_0 = 0) = K_N \int_{E_{\rm low}}^{E_{\rm upp}} E^{-\gamma-1/2}\mathrm{d}E = K_N \begin{cases} \frac{E_{\rm upp}^{-\gamma+0.5} - E_{\rm low}^{-\gamma+0.5}}{0.5-\gamma}, & \gamma \neq 0.5, \\ \frac{1}{\ln\left(\frac{E_{\rm upp}}{E_{\rm low}}\right)}, & \gamma = 0.5, \end{cases} \tag{26}$$

where K_N is the scaling factor from normalization on a beam density. By using N_0 as a free parameter one can calculate K_N for accepted (or derived from observations) lower and upper energy cut-offs, spectral index and some assumptions about how many beam electrons are injected into a flaring atmosphere (see the last two paragraphs in Section 1).

The updated energy spectra found from the CE for the electron density and from the original CE for electron flux are plotted for a few column depths in Fig. 1. It can be seen that the updated solutions for electron densities corrected as proposed by Emslie et al. (2014) still have a steeper decrease at lower energies than the solutions found from the electron flux equation, although this decrease is not as sharp as reported earlier by Dobranskis & Zharkova (2014).

Hence, with the joint efforts of Dobranskis & Zharkova (2014) and Emslie et al. (2014), we have proven that the solution for the electron density N reported by Syrovatskii & Shmeleva (1972) can be only obtained from the CE for the electron density (equation 14) and not from the CE for flux reported in their paper. Furthermore, the resulting spectral index of $-\frac{\gamma+1}{2}$ obtained from the CE for the electron density is confirmed by the inverse problem solutions (Brown 1971), which reflects correctly the variations of electron density during their precipitation in Coulomb collisions. Therefore, initial equation (1) from Syrovatskii & Shmeleva (1972) has to be converted to the equation for the electron density described by equation (14) as proposed by Dobranskis & Zharkova (2014).

The effects of these updated solutions on MES is discussed in Section 4.1 and on HXR emission in Section 5.

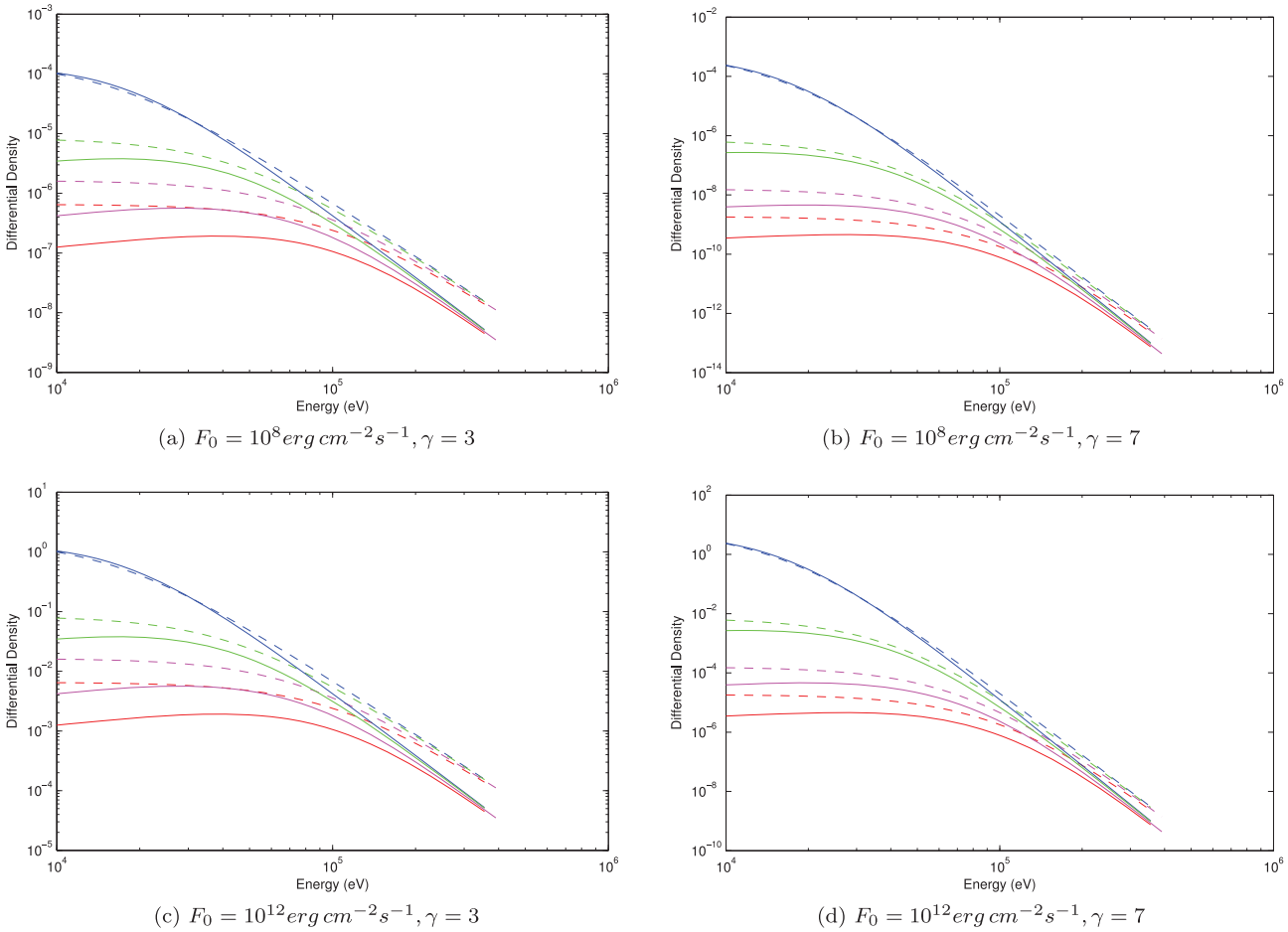

(a) $F_0 = 10^8 erg\,cm^{-2}s^{-1}, \gamma = 3$ (b) $F_0 = 10^8 erg\,cm^{-2}s^{-1}, \gamma = 7$

(c) $F_0 = 10^{12} erg\,cm^{-2}s^{-1}, \gamma = 3$ (d) $F_0 = 10^{12} erg\,cm^{-2}s^{-1}, \gamma = 7$

Figure 1. The variation of electron differential density spectra versus energy plotted for column depths of 1.4×10^{20} (blue), 1.2×10^{21} (green), 4.5×10^{21} (magenta), 1.1×10^{22} (red) and energy range from 10 keV to 1000 keV. The solid lines represent the electron densities N (equation 25) found from the CE for the electron density (equation 14) with correction by Emslie et al. (2014) and the dashed lines are the electron densities (equation 10 derived in Dobranskis & Zharkova 2014) from CE for electron flux.

3 SOLUTIONS OF CE FOR OHMIC LOSSES

3.1 Self-induced electric field and returning beam electrons

Since electron beams carry a substantial electrostatic electric field (Knight & Sturrock 1977; Emslie 1980; Diakonov & Somov 1988), let us now consider precipitation of beam electrons in this self-induced electric field, which is kept steadily distributed over depth for stationary injection of beam electrons (Zharkova & Gordovskyy 2006; Siversky & Zharkova 2009). Hence, let us investigate electron beams steadily injected into a flaring atmosphere from its top with power-law energy distributions and precipitating into denser atmospheric layers while losing their energy in ohmic losses (Zharkova & Gordovskyy 2006).

In this case there are two populations of electrons to be considered: those which continue to precipitate downwards while being braked by the electric field (pitch angle cosine $\mu > 0$ and those, which return back to the corona by this self-induced electric field of the beam (returning electrons with $\mu < 0$). This approach is applied to beam electrons only similar to the one applied by Zharkova & Gordovskyy (2006) and Siversky & Zharkova (2009) that essentially differs from the early approach considering the return current formed from the ambient electrons only (see for example Knight & Sturrock 1977).

With this approach one can notice that an electron beam forms a close electric circuit of electrons moving downwards and upwards 10–100 times per second (Siversky & Zharkova 2009), thus, resolving the long-standing problem of electron number required to account for the number of observed HXR photons. Since a beam electron can make up to 10–100 HXR photons per second while travelling in the electric circuit, then the number of precipitating electrons can be reduced by the factor of 10–100. This means that only about 1–10 per cent of the ambient electrons needs to be accelerated to high energies and injected into a flaring atmosphere (Siversky & Zharkova 2009) to account for HXR emission, instead of the entire ambient plasma of a flaring loop assumed earlier (Brown 1972).

For this model, beam electrons are assumed to lose their energy in ohmic losses (Emslie 1980), and the energy losses are expressed by formula:

$$\frac{dE}{\mu ds} = -e\mathcal{E}, \tag{27}$$

where $\mathcal{E}$ (V cm^{-1}) is the magnitude of the self-induced electrostatic electric field induced by the precipitating electron beams, the pitch angle cosine μ defines a direction of beam electron propagation. For the sake of simplicity, it is assumed that the electron beams injected

at the upper boundary and precipitating downwards ('precipitating' electrons) are described by $\mu = +1$, while the electrons, which are accelerated back to the source in the corona by the self-induced electric field ('returning' electrons) are represented by $\mu = -1$.

3.2 CE for electron flux

By substituting the ohmic energy loss term (equation 27) into the CE (equation 1) one can solve it again analytically by using the method of characteristics (Courant & Hilbert 1962). The resulting general solution obtained for electron flux $F = vN(E, s)$ can be again inverted to obtain the electron density $N = \frac{F}{v}$, in which one can substitute the upper boundary condition (equation 9) to produce the solutions for electron beam differential densities:

$$N(E,s) = K\,(E + e\mathcal{E}s)^{-\gamma-1} \times \Theta\,(E - E_{\rm low} + e\mathcal{E}s)\,\Theta\,(E_{\rm upp} - e\mathcal{E}s - E), \quad \mu = +1, \tag{28}$$

with power-law energy spectra being constrained within the range of $E_{\rm low} < E < E_{\rm upp}$ and the index at the argument $(E + e\mathcal{E}s)$ being higher by 0.5 than in the solutions presented by Zharkova & Gordovskyy (2006).

The same applies to the 'returning' electrons:

$$N(E,s) = K\,(E + e\mathcal{E}s_r)^{-\gamma-1} \times \Theta\,[E_{\rm upp} - E - e\mathcal{E}s_r], \quad \mu = -1, \tag{29}$$

where s_r is the distance traversed by 'returning' electrons (described in details in Sections 3.3.1 and 3.4.2).

In general, the differential spectra presented by the equations above are asymmetric for precipitating (28) and 'returning' (29) beam electrons as defined by the Heavyside function Θ.

3.3 CE for electron density

3.3.1 Analytical CE solutions for a constant electric field

We assume that $E =$ constant, then equation (13) can be used to find direct analytical solutions for electron density N precipitating in purely ohmic losses for both precipitating ($\mu = +1$) and 'returning' ($\mu = -1$) electrons and to compare them with the solutions found from the original CE in Section 3.2.

Let us substitute into the updated CE (equation 13) the expression for ohmic energy losses (equation 27) taking into account that the derivative by E of the term with energy losses (the first term) is equal to zero, since the ohmic energy losses are the same for the electrons with any energies. In result, one can easily obtain the updated CE for ohmic losses in the following form:

$$\frac{\partial N}{\partial s} - e\mathcal{E}\,\frac{\partial N}{\partial E} = \frac{e\mathcal{E}N}{2E}. \tag{30}$$

The equation (30) is a linear inhomogeneous equation PDE, which, contrary to the initial CE, has a free term on the right-hand side, similarly to the collisional case (Dobranskis & Zharkova 2014). Assuming that the values of N are known on some initial curve, the CE (30) can be solved by the method of characteristics (Courant & Hilbert 1962), allowing to derive differential electron density N as a function of linear precipitation depth s and electron energy E for the initial conditions:

$$s(0) = s_0, \qquad E(0) = E_0, \qquad N(0) = N_0, \tag{31}$$

where E and N are functions of s. Then one can derive the characteristic equations for each variable s, E and N obtaining a system of three ordinary differential equations, which are solved as follows:

$$\frac{{\rm d}s}{{\rm d}t} = 1 \;\rightarrow\; s(0) = s_0 \;\rightarrow\; s = t\ldots(+s_0), \tag{32}$$

$$\frac{{\rm d}E}{{\rm d}t} = -e\mathcal{E} \;\rightarrow\; E(0) = E_0 \;\rightarrow\; E = -e\mathcal{E}t + E_0 \rightarrow\; E_0 = E - e\mathcal{E}t, \tag{33}$$

$$\frac{{\rm d}N}{N} = \frac{e\mathcal{E}}{2E}{\rm d}t. \;\rightarrow\; \begin{matrix} u = E_0 - e\mathcal{E}t \\ {\rm d}u = -e\mathcal{E}\,{\rm d}t \end{matrix} \;\rightarrow\; \frac{{\rm d}N}{N} = \frac{{\rm d}u}{2u} \tag{34}$$

For solution of the equation for N the expression for E has to be substituted from equation (33), i.e. $E = E_0 - e\mathcal{E}t$ (where the energy E is treated as a variable and not as a constant, following the correction by Emslie et al. 2014) so that the integration gives the characteristics for N as follows:

$$\ln(N)_{N_0}^{N} = -\frac{1}{2}\ln(u)\,|_{u_0}^{u} \;\rightarrow\; N = N_0 \times (u)^{-1/2} \times (u_0)^{1/2}, \tag{35}$$

using the variables:

$$u(t) = E_0 - e\mathcal{E}t$$

$$u_0(t = 0) = E_0. \tag{36}$$

Hence, by substituting u and u_0 into equation (35) the general solution for N of the CE for ohmic losses can be written as follows:

$$N(E,s) = \Psi\,(E + e\mathcal{E}s) \times E^{-1/2} \times (E + e\mathcal{E}s)^{1/2}. \tag{37}$$

Verification of the solution: similarly to the case for purely collisional energy losses, the general solution of CE for ohmic energy losses can be obtained using the alternative method (Ruderman, private communication). The characteristics of equation (30) are defined by equation (27) with simple solution $E + e\mathcal{E}s =$ constant. Then, following method presented in Section 2.2.2, and making the substitution $\zeta = E + e\mathcal{E}s$ reduces equation (30) to

$$\frac{{\rm d}N}{{\rm d}E}\,|_{\zeta} = -\frac{N}{2E}. \tag{38}$$

The general solution to equation (38) is $N = E^{1/2}F(\zeta)$, where F is an arbitrary function. Introducing $\Psi(\zeta) = \zeta^{1/2}F\zeta$ and recalling the definition of ζ, the general solution of CE for ohmic energy losses is produced:

$$N(E,s) = \Psi\,(E + e\mathcal{E}s) \times E^{-1/2} \times (E + e\mathcal{E}s)^{1/2}, \tag{39}$$

which is exactly the same as general solution (37).

The final solution for differential densities: let us now substitute the initial energy spectrum at the top boundary (equation 9) into the general solution (equation 37). This results in the following differential density of precipitating electron beams losing their energy in purely ohmic losses:

$$N(E,s) = K_N E^{-1/2}(E + e\mathcal{E}s_i)^{-\gamma} \times \Theta\,[E + e\mathcal{E}s_i - E_{\rm low}]\,\Theta\left[E_{\rm upp} - E - e\mathcal{E}s_i\right], \quad \mu = +1, \tag{40}$$

where the scaling factor K_N is estimated through normalization on a beam density N_0 (equation 26) at the top boundary by equating it to the ambient plasma density or its fraction.

The CE solution (40) is similar to the one obtained by Zharkova & Gordovskyy (2006, their equation 11), however it can be only obtained by solving the CE for electron density N (using the same analytical approach as proposed by Dobranskis & Zharkova 2014). As a result, the spectral index γ obtained from solution for the electron density (equation 40), will differ by 1 from the solution presented in equation (28) found from CE solution for electron flux, and it does not have a factor of $E^{-1/2}$.

The solution for returning beam electrons ($\mu = -1$) moving back to the corona by a constant electric field induced by a precipitating beam can be written as follows:

$$N(E,s) = K_N E^{-1/2}(E + e\mathcal{E}s_r)^{-\gamma} \times \Theta\left[E_{\rm upp} - E - e\mathcal{E}s_r\right], \quad \mu = -1, \tag{41}$$

where s_r is expressed as follows:

$$s_r = s_\mathcal{E} - s_i. \tag{42}$$

Here, $s_\mathcal{E} = \frac{E}{e\mathcal{E}}$ is the electric stopping depth of electron with energy E (Zharkova & Gordovskyy 2006) and s_r is the distance travelled by returning electrons from their stopping depth upwards to the corona to a distance s_i measured from the top.

In the case of continuous injection of precipitating electrons they will keep producing their electrostatic electric field, so that the beam electrons, which stopped become accelerated back to the source. During the motion upwards they can gain the energy as $E_i = E_0 + e\mathcal{E}s_r$, where E_0 refers to the initial energy (which is 0 for 'returning' electron with energy E) and $e\mathcal{E}s_r$ is the energy gain term.

It can be noted that equation (41) does not have the lower energy restriction, since it is assumed that the beam electrons lose their energy completely before starting moving by their self-induced electric field back to the injection point in the corona.

Since precipitating beam electrons stop at their individual stopping depths defined by their initial energies, it is important to look at a range of stopping depths (or energies) of the whole set of 'returning' electrons present at a given depth s_i rather than a single one, in order to obtain the correct differential density spectra or returning electrons.

3.3.2 Analytical solutions of CE for a variable electric field

As shown by the earlier numerical simulations (Zharkova & Gordovskyy 2006), the self-induced electric field varies significantly through a flaring atmosphere, being nearly constant in the corona and dropping sharply with depth at deeper atmospheric depths in the chromosphere (Zharkova & Gordovskyy 2006; Siversky & Zharkova 2009). In order to account for these complex depth variations of the self-induced electric field, let us use the following formula from Zharkova & Gordovskyy (2006):

$$\mathcal{E} = \mathcal{E}_0 \left(\frac{s}{s_t}\right)^{-k}, \tag{43}$$

where $\mathcal{E}_0$ – the magnitude of a constant electric field, s – a linear precipitation depth associated with the column depth and ambient plasma density as $s \simeq \xi \backslash n$, the s_t is a turning depth, after which the self-induced electric field starts decreasing ($s \geq s_t$) and k is the index of electric field distribution, which defines the slope of the electric field drop with depth.

In this case of the variable electric field the ohmic energy losses can be found by integrating equation (43) by a precipitation depth s by taking into account that the electric field is constant until some precipitation depth s_t, called a 'turning depth', after which the field starts to decrease as per equation (43). Then, the losses in a variable electric field can be expressed in the following way:

$$e\mathcal{E}_0 s_t + \int_{s_t}^{s_i} e\mathcal{E}_0 \left(\frac{s}{s_t}\right)^{-k} {\rm d}s = e\mathcal{E}s_t \times \begin{cases} [1 + \ln(s_i/s_t)], & k = 1, \\ \left[1 + \frac{s_i^{1-k} - s_t^{1-k}}{s_t^{1-k}(k-1)}\right], & k \neq 1. \end{cases}$$

The first term on the right-hand side represents the losses in a constant electric field before the turning depth s_t and the second term – in the variable electric field at the depths beyond s_t. By substituting these losses into the formula for differential density (equation 41), the updated CE solutions for electrons precipitating in the variable electric field can be written as follows:

$$N(E,s) = K_N\sqrt{E}\,[E + e\mathcal{E}s_t + e\mathcal{E}s_t \ln(s_i/s_t)]^{-\gamma} \times \Theta\,[E + e\mathcal{E}s_t + e\mathcal{E}s_t \ln(s_i/s_t) - E_{\rm low}] \times \Theta\left[E_{\rm upp} - E - e\mathcal{E}s_t - e\mathcal{E}s_t \ln(s_i/s_t)\right], \quad k = 1. \tag{45}$$

$$N(E,s) = K_N\sqrt{E}\left[E + e\mathcal{E}s_t\left(1 + \frac{s_i^{1-k} - s_t^{1-k}}{s_t^{1-k}(k-1)}\right)\right]^{-\gamma} \times \Theta\left[E + e\mathcal{E}s_t\left(1 + \frac{s_i^{1-k} - s_t^{1-k}}{s_t^{1-k}(k-1)}\right) - E_{\rm low}\right] \times \Theta\left[E_{\rm upp} - E - e\mathcal{E}s_t\left(1 + \frac{s_i^{1-k} - s_t^{1-k}}{s_t^{1-k}(k-1)}\right)\right], \quad k \neq 1. \tag{46}$$

3.4 Differential energy spectra

3.4.1 Precipitating electrons

The differential spectra of beam electrons losing their energy in purely ohmic losses (equation 40) obtained from the CE solutions for the electron density are presented in Fig. 2 for a moderately intense and hard beams ($F_0 = 10^{10}$ erg cm^{-2} s^{-1}, $\gamma = 3$, top row), for soft beams ($F_0 = 10^{10}$ erg cm^{-2} s^{-1}, $\gamma = 7$, bottom row). The electron energies range within $E_{\rm low} = 16$ and $E_{\rm upp} = 384$ keV. The results presented in Figs 2(a) and (c) are obtained for the constant electric field of $\mathcal{E}_0 = 3.0 \times 10^{-6}$ V cm^{-1} for $\gamma = 3$ and $\mathcal{E}_0 = 1.0 \times 10^{-5}$ V cm^{-1} for $\gamma = 7$. The plots in Figs 2(b) and (d) are calculated for a variable electric field having at upper atmosphere levels the same initial values as above and falling with depth parabolically ($k = 2$) after the turning depth $s_t = 6.4 \times 10^8$ cm.

As expected, the solution (equation 37) found from CE for the electron density has an additional term $(E + e\mathcal{E}s)^{1/2}$ compared to the solution of CE for electron flux, which results in the increase of differential density of precipitating electrons at a given depth. Similarly to the collisional losses, hard beams (Figs 2a and b) keep flatter distribution than softer ones (Figs 2a and b), thus, having larger differential densities at the similar precipitation depths and thus reaching deeper layers. Indeed, for variable electric field the 'electric' stopping depth $s_\mathcal{E} = E \backslash e\mathcal{E}$, at which lower energy electrons lose their energy completely, occurs at higher atmospheric levels in the corona or upper chromosphere (Zharkova & Gordovskyy 2006, Table 1), often exceeding the collisional ones for more powerful

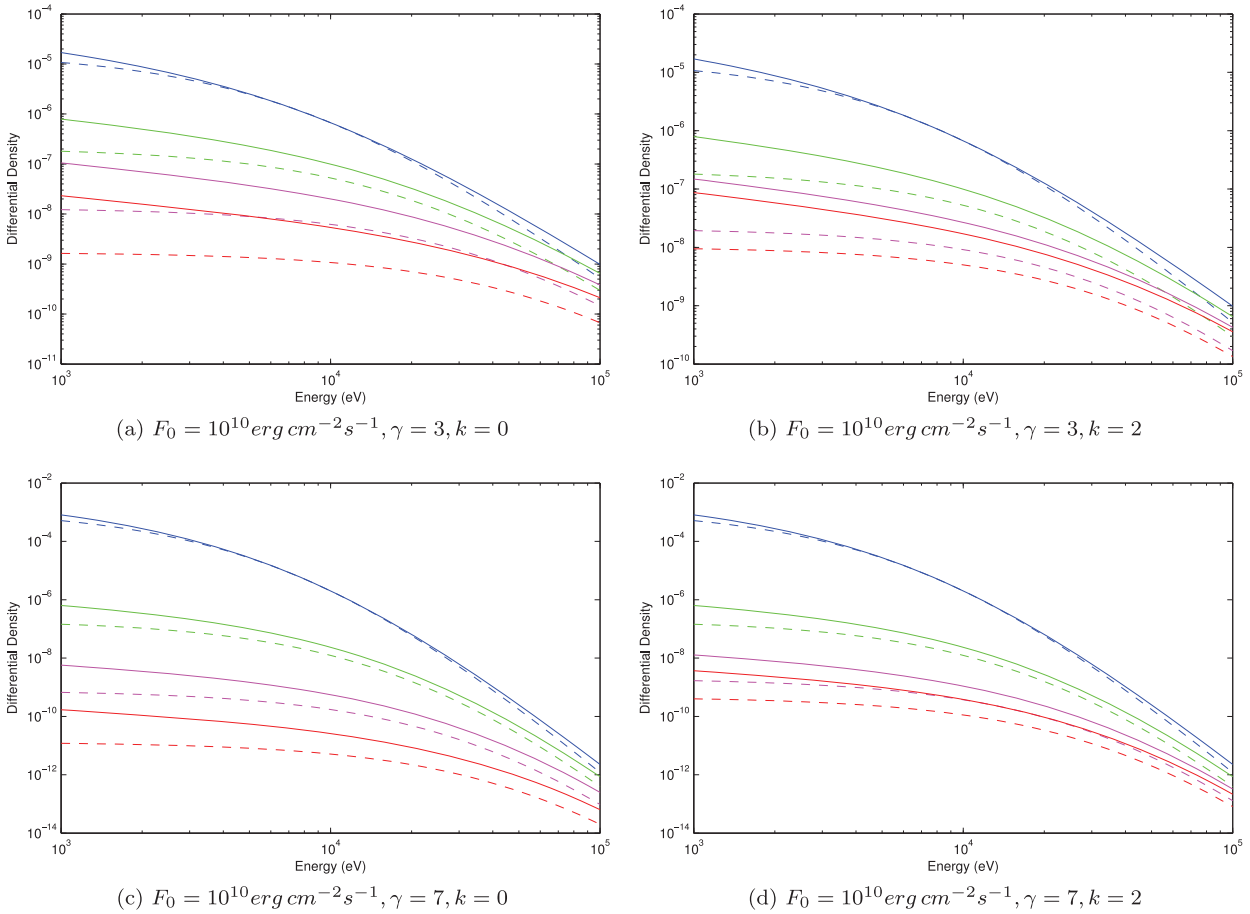

(a) $F_0 = 10^{10} erg\,cm^{-2}s^{-1}, \gamma = 3, k = 0$ (b) $F_0 = 10^{10} erg\,cm^{-2}s^{-1}, \gamma = 3, k = 2$

(c) $F_0 = 10^{10} erg\,cm^{-2}s^{-1}, \gamma = 7, k = 0$ (d) $F_0 = 10^{10} erg\,cm^{-2}s^{-1}, \gamma = 7, k = 2$

Figure 2. The variations of beam electron differential density versus energy calculated, at the precipitation depths (s) of 1.6×10^8 cm (blue), 4.8×10^8 cm (green), 9.6×10^8 cm (magenta) and 16.0×10^8 cm (red). The solid lines represent the results of the updated CE (equation 40) and the dashed lines correspond to the original approach (equation 28) by Zharkova & Gordovskyy (2006).

Table 1. Variation of the spectral indices for $F_0 = 10^{12}$ erg cm^{-2} s^{-1}, for Fokker–Planck, original CE and updated CE for Coulomb collisions.

Initial electron index	$\gamma = 3$		$\gamma = 7$	
Approach \ Energy	< 40keV	> 40keV	< 40keV	> 40keV
MES	$\gamma_{MES} = 1$		$\gamma_{MES} = 5$	
HXR (Fokker–Planck)	$\delta_1 = 1.7$	$\delta_2 = 2.5$	$\delta_1 = 5.3$	$\delta_2 = 5.4$
HXR (Original CE)	$\delta_1 = 1.5$	$\delta_2 = 2.4$	$\delta_1 = 5.1$	$\delta_2 = 5.2$
HXR (Updated CE)	$\delta_1 = 1.8$	$\delta_2 = 2.6$	$\delta_1 = 5.3$	$\delta_2 = 5.2$

electron beams. This leads to an increase of the electron density at lower energies. The comparison of differential densities (Fig. 2a) at 1 keV energy, showed that the updated CE densities at the precipitation depth $s = 16.0 \times 10^8$ cm are approximately three times higher, while at the depth $s = 4.8 \times 10^8$ cm it is 1.7 times higher.

Furthermore, softer beams (Fig. 2c) induce a higher electrostatic electric field than the hard ones (Fig. 2a), thus shifting up electron stopping depths closer to the injection point. Slightly different scenario occurs when the variable electric field starts to decrease after the turning depth located at $s = 6.4 \times 10^8$ cm (Figs 2b and d). By comparing Figs 2(a) and (b), one can see that the differential density spectra for precipitation depths 9.6×10^8 cm (magenta) and 16.0×10^8 cm (red), obtained for variable electric field, have become steeper. Therefore, due to a decrease of the electric field at these depths, precipitating electrons have smaller energy losses and less steep flattening. At the same time, for harder beams the electric stopping depth is shifted deeper into the atmosphere, because they induce a lower electric field, thus, revealing a smaller flattening towards lower energies (Figs 2a and b).

3.4.2 *Returning electrons*

The plots of differential densities versus energies for 'returning' electrons formed by a constant (left-hand column, $k = 0$) and variable (right-hand column, $k = 2$) electric fields are presented in Fig. 3. The differential spectra of 'returning' electrons presented in Fig. 3 are obtained for the same parameters as for precipitating electrons in Section 3.4.1. It was assumed that the electrons become returning (and accelerated) from the precipitation depths ranging from 16.0×10^8 cm to 40.0×10^8 cm, which are the stopping 'electric' depths for electrons with the lower and upper cut-off energies, respectively.

It is evident that in the presence of self-induced electric field, the beam electrons precipitate to some layer in the atmosphere before losing all their energy, and higher energy electrons reach deeper layers than the lower energy ones. Then, because of the action of electrostatic electric field, these stopped electrons begin to move upwards to the source, while gaining the energy from this electric field by traversing the distances between $s_\mathcal{E}$ and s_r. The maximum energy gains at given depth s_r is limited to the

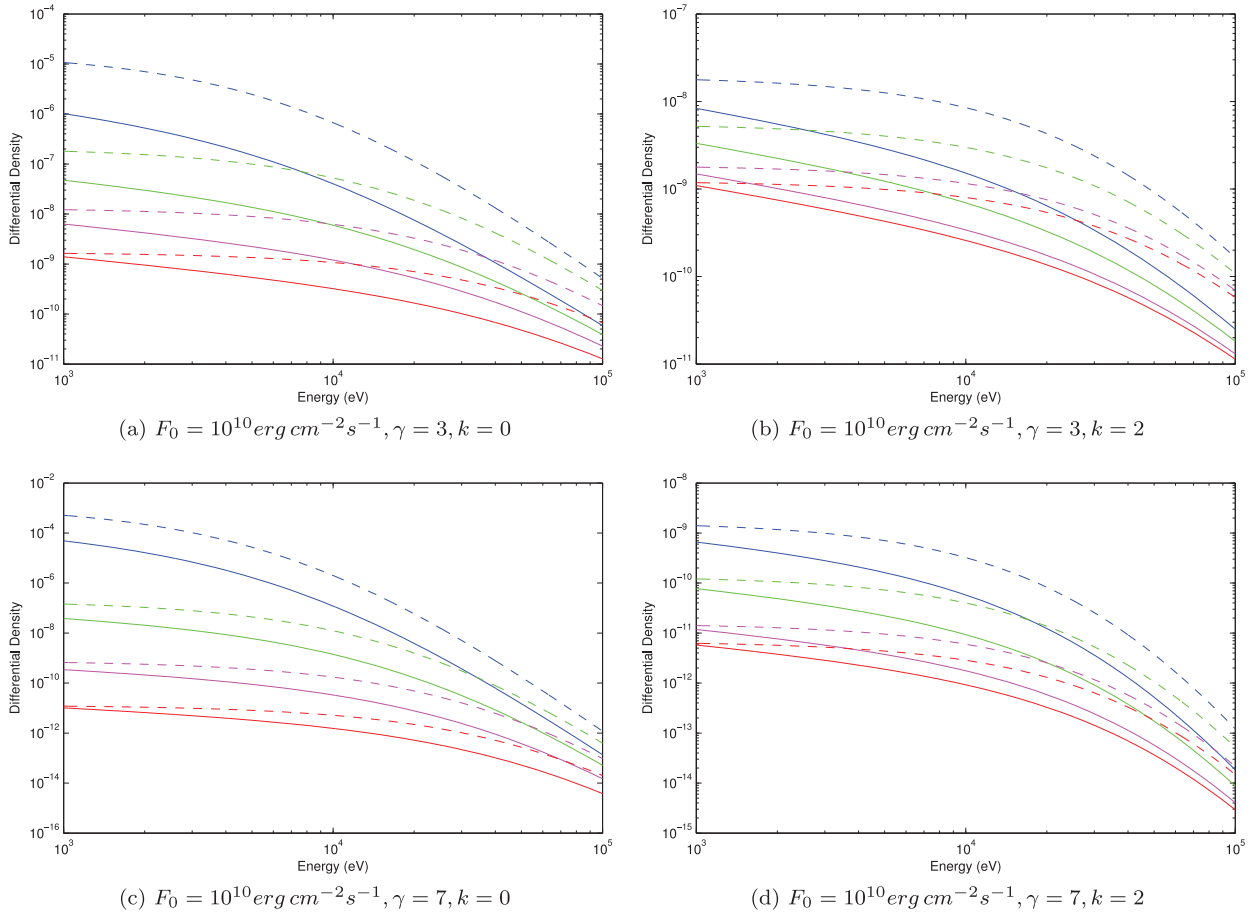

(a) $F_0 = 10^{10} erg\,cm^{-2}s^{-1}, \gamma = 3, k = 0$ (b) $F_0 = 10^{10} erg\,cm^{-2}s^{-1}, \gamma = 3, k = 2$

(c) $F_0 = 10^{10} erg\,cm^{-2}s^{-1}, \gamma = 7, k = 0$ (d) $F_0 = 10^{10} erg\,cm^{-2}s^{-1}, \gamma = 7, k = 2$

Figure 3. The variations of differential densities of 'returning' electrons for the updated (solid line) and original (dashed line) solutions (Zharkova & Gordovskyy 2006), respectively. Simulation parameters not stated in the legend are as follows: constant or initial electric field $\mathcal{E}_0$ value – 5×10^{-5} V cm^{-1}, differential densities are shown at the same precipitation depths as in Fig. 2. The lowest precipitation depth, from which electrons, begin to accelerate back towards the source is 40×10^8 cm (where 200 keV electrons precipitating in a constant electric field lose all energy).

$E_{\rm upp} = e\mathcal{E}s_r$ (equation 41). Thus, the energy gained by returning electrons, depends on the 'electric' stopping depth $s_{\mathcal{E}}$, which is associated with the initial electron energy.

The updated solution of CE for 'returning' electrons (equation 41) has harder spectral index $-\gamma$, compared to $-\gamma - 1$ derived from the original solution (equation 29). The differential density distribution follows a negative slope with a flattening at energies below 10 keV, which becomes more pronounced at lower atmospheric depths.

The energy gained by returning electrons is proportional to the traversed distance travelled by electrons from their electrical stopping depth for a given electric field magnitude. As a result, the number of returning electrons accelerated in the constant electric field (Figs 3a and c), increases significantly at any precipitation depth, reaching the maximum at the upper boundary. However, in case of a variable electric field (Figs 3b and d), only a small number of electrons are accelerated at the lower column depths. Returning electrons gain more energy with every precipitation depth having smaller gains in a variable electric field and larger gains in a higher constant electric field.

4 MEAN ELECTRON SPECTRA

Let us explore the effect of the proposed CE updates for collisional and ohmic losses on MES.

4.1 MES for collisional losses

MES for collisional losses can be calculated by using the corrected (25) and compared with the original (10) solutions for CE equation for the electron density in the following way:

$$\begin{aligned}\bar{F}(E) &= K\sqrt{\frac{2E}{m}}\int_0^{\infty}\left(E^2+2a\xi\right)^{-\frac{\gamma+1}{2}} \times E^{1/2}\mathrm{d}\xi \\ &= KE\sqrt{\frac{2}{m}}\int_0^{\infty}\left(E^2+2a\xi\right)^{-\frac{\gamma+1}{2}}\mathrm{d}\xi \\ &= \frac{KE}{2a}\sqrt{\frac{2}{m}}\int_{E^2}^{E^2_{\rm upp}} u^{-n}\mathrm{d}u \\ &= \frac{KE}{2a}\sqrt{\frac{2}{m}}\frac{E^{2-2n}}{n-1}, \quad \text{for } E \ll E_{\rm upp}, \end{aligned} \tag{47}$$

$$\begin{aligned}\bar{F}(E) &= K\sqrt{\frac{2E}{m}}\int_0^{\infty}\left(E^2+2a\xi\right)^{-\gamma/2}\mathrm{d}\xi \\ &= \frac{K}{2a}\sqrt{\frac{2E}{m}}\int_{E^2}^{E^2_{\rm upp}} u^{-n_1}\mathrm{d}u \\ &= \frac{K}{2a}\sqrt{\frac{2E}{m}}\frac{E^{2-2n_1}}{n_1-1}, \quad \text{for } E \ll E_{\rm upp}, \end{aligned} \tag{48}$$

where $u = E^2 + 2a\xi$. Meanwhile the integration limits E and $E_{\rm upp}$ originate from the lower and upper energy cut-off's imposed on the solved CE via Heavyside step functions ($\Theta(\sqrt{E^2 + 2a\xi} - E_{\rm low})$ and $\Theta(E_{\rm upp} - \sqrt{E^2 + 2a\xi})$). The energy of precipitating electrons E is constrained between two limits as $E_{\rm low} \leq E \leq E_{\rm upp}$, where E is a variable energy, while $E_{\rm low}$ and $E_{\rm upp}$ have constant value.

The correct lower integration limit is obtained from the first Heavyside step function, which will produce 1 for all positive outcomes, or, if relation below

$$E^2 + 2a\xi \geq E_{\rm low}^2, \tag{49}$$

is true. This relation can be further simplified by setting the column depth ξ to 0, resulting in $E^2 \geq E_{\rm low}^2$, which implies that lower integration limit should be variable energy E^2.

Similar approach is used to find the upper integration limit. This time second Heavyside step function is investigated, and produce the relation

$$E_{\rm upp}^2 \geq E^2 + 2a\xi, \tag{50}$$

which implies that the upper integration limit should be $E_{\rm upp}^2$.

Once integration limits are set correctly, integration for column depth is done, producing solutions (47) and (48), where the spectral index n for the corrected solution (25) is defined as

$$n = \frac{\gamma + 1}{2}, \tag{51}$$

while for the original solution it is equal to

$$n_1 = \frac{\gamma}{2}. \tag{52}$$

The substitution of n and n_1 into the formulas (47) and (48) for MES results in the following dependence of MES on energy:

(i) for the updated solution (25) from CE (14) for electron density,

$$\begin{aligned}\bar{F}(E) &= \frac{K_N E}{2a}\sqrt{\frac{2}{m}}\frac{E^{2-(\gamma+1)}}{(\gamma+1)/2-1} \\ &= \frac{K_N E}{2a}\sqrt{\frac{2}{m}}\frac{E^{-(\gamma-1)}}{(\gamma-1)/2} = {\rm CE}^{-(\gamma-2)};\end{aligned} \tag{53}$$

(ii) for the original solution (10) from CE for electron flux,

$$\begin{aligned}\bar{F}(E) &= \frac{K}{2a}\sqrt{\frac{2E}{m}}\frac{E^{2-\gamma}}{\gamma/2-1} \\ &= \frac{K}{2a}\sqrt{\frac{2E}{m}}\frac{E^{-(\gamma-2)}}{(\gamma-2)/2} = C_1 E^{-(\gamma-2.5)}.\end{aligned} \tag{54}$$

4.2 MES for ohmic losses

4.2.1 The original CE for electron flux

The differential spectra for purely ohmic losses discussed in the previous Section 3.4 can be used to derive the MES, which were previously estimated from the original CE solution for electron flux by Zharkova & Gordovskyy (2006). The MES of an electron beams precipitating in the constant electric field can be derived by integration of the corresponding differential densities (equation 28) for precipitation depths in the range from 0 to infinity (in the case of ohmic energy losses, the lower and upper integration limits are replaced with E and $E_{\rm upp}$, respectively, using the same method as described in the previous Section 4.1) as follows:

$$\begin{aligned}\bar{F}(E) &= \int_0^\infty vN(E,s){\rm d}s \\ &= \sqrt{\frac{2}{m}} \times \frac{K}{e\mathcal{E}\,(\gamma - 0.5)} E^{-\gamma+0.5}.\end{aligned} \tag{55}$$

4.2.2 The updated MES solutions for ohmic losses

The updated CE solutions for differential density (equation 40) of precipitating electron beams, presented in Section 3.3.1, can also be integrated over a linear precipitation depth to produce the updated MES solutions for ohmic losses (equation 40) as follows:

$$\bar{F}(E) = K_N\sqrt{\frac{2}{m}}\int_0^\infty (E + e\mathcal{E}s)^{-\gamma}\,{\rm d}s. \tag{56}$$

Therefore, after successful integration, solution for ohmic MES at energies above $E_{\rm low}$ is obtained:

$$\bar{F}(E) = \frac{K_N}{e\mathcal{E}}\sqrt{\frac{2}{m}}\left(\frac{E_{\rm upp}^{1-\gamma}}{1-\gamma} - \frac{E^{1-\gamma}}{1-\gamma}\right) \quad \text{for} \quad E \ll E_{\rm upp}, \tag{57}$$

The solution above can be further simplified to the following form:

$$\bar{F}(E) = \frac{K_N}{e\mathcal{E}\,(\gamma-1)}\sqrt{\frac{2}{m}}E^{-\gamma+1} \quad \text{for} \quad E \ll E_{\rm upp}. \tag{58}$$

As a result, the MES solution obtained by integration of the updated CE for ohmic losses (equation 40) for linear precipitation depth, has a harder spectral index $-\gamma + 1$ (equation 58) compared to the index of $-\gamma + 0.5$ derived from the original CE solutions for electron flux (equation 55).

5 HXR INTENSITY

The updated CE for purely collisions (Section 2.2.2) can be used to evaluate the resulting HXR bremsstrahlung emission. Similarly to Dobranskis & Zharkova (2014), the differential densities, obtained for purely collisional loss are used to define the distribution function $f(E,\xi) = \frac{N(E,\xi)}{N(E,0)}$. For comparison, the similar distribution functions $f_N(E,\xi)$ integrated over pitch angle cosines are obtained for the same beam parameters from the numerical Fokker–Planck approach (Siversky & Zharkova 2009).

In order to estimate HXR intensity I, the corresponding distribution functions f_N are integrated by azimuthal angles, pitch angle cosines, photon energy and column depth as follows:

$$I(\varepsilon) = 2\pi A_x K\int_{\xi_{\rm min}}^{\xi_{\rm max}}\int_\varepsilon^\infty\int_{-1}^1 f(\xi,\eta,\mu)\,\eta\sigma^H(\eta,\varepsilon)\,{\rm d}\mu{\rm d}\eta{\rm d}\xi, \tag{59}$$

where ξ is column depth, η is the photon energy, μ is the pitch angle cosine, ε is a dimensionless photon energy $h\nu/E_0$ and $A_x = \frac{S}{4\pi R}\frac{2E}{m_e}$, where S defines area of a flare and R is a distance to the observer ($\approx$ 1 au). In equation (59), the relativistic cross-sections defined by Bai & Ramaty (1978) and updated by Zharkova, Kuznetsov & Siversky (2010) are used.

Now let us use the updated differential densities of precipitating beam electrons derived for purely Coulomb collisions in Section 2.2 to calculate the intensities of HXR bremsstrahlung emission presented in Fig. 4. The HXR intensities of precipitating electrons are compared for the three following approaches: (1) the original CE for electron flux (red lines), (2) the updated CE for purely Coulomb

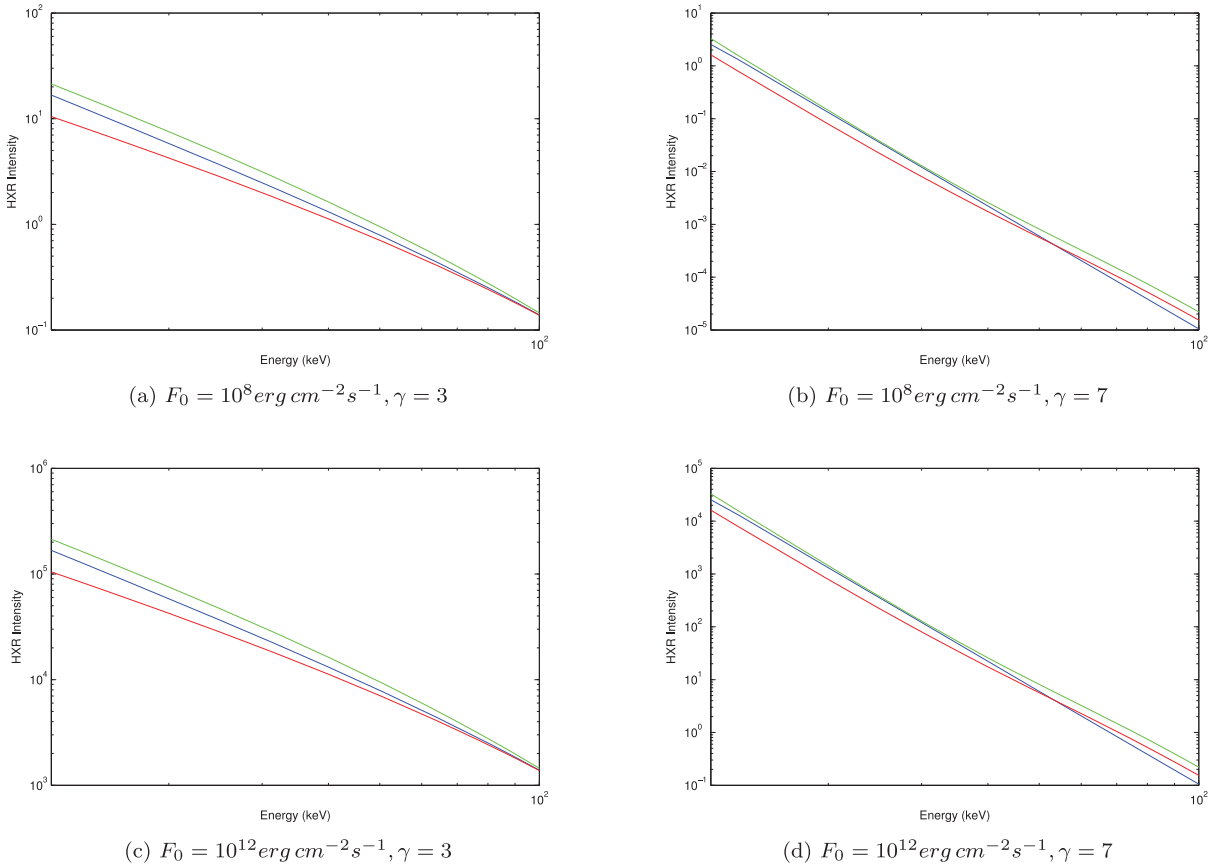

(a) $F_0 = 10^8 erg\,cm^{-2}s^{-1}, \gamma = 3$ (b) $F_0 = 10^8 erg\,cm^{-2}s^{-1}, \gamma = 7$

(c) $F_0 = 10^{12} erg\,cm^{-2}s^{-1}, \gamma = 3$ (d) $F_0 = 10^{12} erg\,cm^{-2}s^{-1}, \gamma = 7$

Figure 4. HXR intensity in relative units, obtained from the original CE (red lines), the updated CE (green lines) solution for purely Coulomb collisions and the numerical Fokker–Planck solution (blue lines).

collisions (Dobranskis & Zharkova 2014, green lines) and (3) the numerical FP solution for Coulomb collisions with pitch angle scattering (Siversky & Zharkova 2009, blue crosses). The parameters of electron beams are as follows: the initial energy fluxes of $F_0 = 10^{10}$ (top plots) and 10^{12} erg cm^{-2} s^{-1} (bottom plots), the spectral indices $\gamma = 3$ (left-hand column plots) and 7 (right-hand column plots); the lower and upper energy cut-offs $E_{\rm low} = 12$ keV and $E_{\rm upp} = 12$ MeV, respectively.

In the case of harder electron beams ($\gamma = 3$, Figs 4a and c), at the energies below 40 keV, the updated CE solution produce a slightly harder distribution, comparing to FP solution. This can be explained by partial pitch angle scattering of lower energy electrons considered in FP approach while in the CE approach the contribution of pitch angle scattering was calculated as a full integral giving higher electron densities and higher HXR emission at lower energies where the pitch angle scattering is the most significant (Siversky & Zharkova 2009).

Although, it can be seen that almost identical distributions are obtained for softer electron beams ($\gamma = 7$, Figs 4b and d), while for lower spectral indices δ_1 (at energies <40 keV) are practically identical and certainly correlate with FP results better than the results produced by the original CE, which differ by 0.2, being harder $\delta_1 = 5.1$ in original case comparing to softer $\delta_1 = 5.3$ for FP solution (Table 1). This better fit is likely to be a consequence of larger energy losses in each process of electron scattering on the ambient particles when pitch angle scattering becomes less essential.

Therefore, the results presented in Fig. 4 and Table 1 reveal that the HXR intensities for electron beams obtained from the updated CE solution for the electron density (green line) have a closer fit to the ones obtained from the numerical Fokker–Planck solution (blue line) than those derived from the CE for electron flux. Given the fact that only the updated solutions are used by the *RHESSI* users utilizing the classic collisional solutions(Brown 1971; Syrovatskii & Shmeleva 1972), this finding confirms acceptable approximation of analytical approach for purely collisional losses derived from the updated CE equation.

However, here we do not compare the HXR photon spectra with those observed because for a correct comparison the effect of ohmic losses should be considered simultaneously with collisional losses as proven by numerous FP simulations of HXR intensity and polarization (Zharkova et al. 1995, 2010, 2011; Zharkova & Gordovskyy 2006; Siversky & Zharkova 2009). This will be a scope of the forthcoming paper.

6 DISCUSSION AND CONCLUSIONS

In this study, we corrected the previous analytical solutions (Dobranskis & Zharkova 2014) for electron densities (normalized on electron density) for purely collisional losses found from the updated CE following the correction proposed by Emslie et al. (2014) and derived the updated analytical solutions for purely ohmic losses for both precipitating and returning electrons.

The solutions of CE for the electron density presented in Dobranskis & Zharkova (2014) are corrected by eliminating a mistake in the density characteristic pointed out by Emslie et al. (2014). The corrected solutions for purely collisions result in the electron

beam differential densities having energy spectra with the index of $-(\gamma + 1)/2$ at the argument $(E^2 + 2a\xi)$ depending on both energy E and column density ξ that coincides with the index derived from the inverse problem solution by Brown (1971). It is evident that this index is lower by 1/2 than index of $-\gamma/2$ obtained from CE for electron flux. This correction, in turn, leads to a change in the index of MES from $-(\gamma - 2, 5)$ (for CE for flux) to $-(\gamma - 2.0)$ (for CE for electron density).

This correction highlighted the fact that for obtaining the energy spectra of electron precipitating in purely collisions used by the *RHESSI* community for the past four decades one needs to use the updated CE for the electron density and not the one for electron flux.

The similar characteristics approach is applied for solution of the CE for the electron density for the case of purely ohmic losses in an electric field induced by the electron beam itself. We consider the two populations of electrons: those which continue to precipitate downwards and those of return current, which are returned by this self-induced electric field of the beam back to the top. This is the approach similar to Zharkova & Gordovskyy (2006) and Siversky & Zharkova (2009) that essentially differs from the early approaches considering a return current to be formed from the ambient electrons only (see for example Knight & Sturrock 1977).

The approach considering returning electrons as a fraction of the population of precipitating electrons which are turned to pitch angles above 90° was suggested earlier by Siversky & Zharkova (2009), who established from the time-dependent Fokker–Planck simulations that an electron beam forms a close electric circuit from the electrons moving downwards to the photosphere and upwards to the corona; and each electron can make about 10–100 journeys per second.

This approach of the return current formed by high-energy electrons themselves, resolves the long-standing problem of the electron number required to account for number of the observed HXR photons in flares. Since the beam electron can make up to 10–100 HXR photons per second while travelling in the circuit, then the number of precipitating electrons can be reduced by the factor 10–100 meaning that only up to 10 per cent of the ambient electrons needs to be accelerated and injected in a flaring atmosphere (Siversky & Zharkova 2009).

The updated CE solution for electron beams precipitating in purely ohmic losses, is shown to have the additional exponential term of $E + e\mathcal{E}s$ with power of 1/2, compared to the original CE for electron flux, resulting in a decrease of spectral index from $-\gamma - 1$ (for CE for flux) to $-\gamma$ (for CE for electron density) leading to flattening of differential density spectra. The effect varies with a linear precipitation depth, being minimal closer to the injection source at the upper boundary in the corona, while deviating much stronger from the original CE results at the deeper atmospheric levels. For example, a comparison of differential densities at 1 keV energy showed that at the precipitation depth $s = 16.0 \times 10^8$ cm the updated CE results will be approximately three times higher, while at depth $s = 4.8 \times 10^8$ cm it will be 1.7 times higher, than from original CE solution.

For returning electrons, in a constant electric field occurring at the coronal and upper chromosphere levels (Zharkova & Gordovskyy 2006), the updated CE also produces an additional term with a positive power of E leading to the differential density distributions becoming flatter; this effect increases at greater atmospheric depths. The energy gained by returning electrons is proportional to the traversed distance upwards from a bottom of the atmosphere and the electric field magnitude at a given depth. As a result, the number of returning electrons accelerated in a constant electric field, would increase significantly with every reverse precipitation depth (from the bottom to the top), reaching its maximum at the upper boundary. While in the case of variable electric field, electrons are found to gain much less energy in this electric field and, as a consequence, their differential density at all precipitation depths becomes consistently smaller than for a constant electric field.

MES derived from the updated CE for electrons with ohmic losses are found to have spectral indices $-\gamma + 1$, which are higher by 0.5 than for the original CE solutions $(-\gamma + 0.5)$ for electron flux, similar to those found for collisional losses (Dobranskis & Zharkova 2014). This evidently leads to mean electron densities with higher magnitudes at every precipitation depth found from the CE for electron density compared to the CE for electron flux.

Also the electron energy spectra obtained from the updated CE solution for Coulomb collisions are shown to produce softer HXR photon spectra than the original CE for electron flux which incidentally fit closer the calculated HXR spectra obtained from the numerical Fokker–Planck solution. Slight discrepancies occur for electrons at lower energies for harder electron beams, and at higher energies for softer electron beams that can be a consequence of partial pitch angle scattering considered in FP approach (Siversky & Zharkova 2009) also pointed by Emslie et al. (2014).

However, for a more accurate comparison of HXR photon spectra with those observed by *RHESSI* the effect of ohmic losses should be considered simultaneously with collisional losses that will be a scope of the forthcoming paper.

ACKNOWLEDGEMENTS

The authors wish to acknowledge that this research is funded by the Science Technology and Facility Council (STFC) project ST/J5000938/1. The authors would like to express their deepest gratitude to Prof Michael Ruderman (Sheffield University, UK) for useful discussion and very constructive comments, from which the paper strongly benefited.

REFERENCES

Bai T., Ramaty R., 1978, ApJ, 219, 705
Brown J. C., 1971, Sol. Phys., 18, 489
Brown J. C., 1972, Sol. Phys., 26, 441
Brown J. C., Emslie A. G., Holman G. D., Johns-Krull C. M., Kontar E. P., Lin R. P., Massone A. M., Piana M., 2006, ApJ, 643, 523
Conway A. J., Brown J. C., Eves B. A. C., Kontar E., 2003, A&A, 407, 725
Courant R., Hilbert D., 1962, Methods of Mathematical Physics, Vol. 2. Interscience, New York
Diakonov S. V., Somov B. V., 1988, Sol. Phys., 116, 119
Dobranskis R. R., Zharkova V. V., 2014, ApJ, 788, 42
Emslie A. G., 1980, ApJ, 235, 1055
Emslie A. G., Holman G. D., Litvinenko Y. E., 2014, ApJ, 792, 5
Haydock E. L., Brown J. C., Conway A. J., Emslie A. G., 2001, Sol. Phys., 203, 355
Holman G. D., Sui L., Schwartz R. A., Emslie A. G., 2003, ApJ, 595, L97
Holman G. D. et al., 2011, Space Sci. Rev., 159, 107
Knight J. W., Sturrock P. A., 1977, ApJ, 218, 306
Kontar E. P., Brown J. C., 2006, ApJ, 653, L149
Kontar E. P., Brown J. C., McArthur G. K., 2002, Sol. Phys., 210, 419
Krucker S. et al., 2008, A&AR, 16, 155
Leach J., Petrosian V., 1981, ApJ, 251, 781
Lin R. P. et al., 2003, ApJ, 595, L69
McClements K. G., 1992, A&A, 253, 261
Massone A. M., Emslie A. G., Kontar E. P., Piana M., Prato M., Brown J. C., 2004, ApJ, 613, 1233

Piana M., Massone A. M., Kontar E. P., Emslie A. G., Brown J. C., Schwartz R. A., 2003, ApJ, 595, L127
Siversky T. V., Zharkova V. V., 2009, A&A, 504, 1057
Sui L., Holman G. D., Dennis B. R., 2005, ApJ, 626, 1102
Sui L., Holman G. D., Dennis B. R., 2007, ApJ, 670, 862
Syrovatskii S. I., Shmeleva O. P., 1972, SvA, 16, 273
Zharkova V. V., Gordovskyy M., 2005, A&A, 432, 1033
Zharkova V. V., Gordovskyy M., 2006, ApJ, 651, 553
Zharkova V. V., Brown J. C., Syniavskii D. V., 1995, A&A, 304, 284
Zharkova V. V., Kuznetsov A. A., Siversky T. V., 2010, A&A, 512, A8
Zharkova V. V., Meshalkina N. S., Kashapova L. K., Kuznetsov A. A., Altyntsev A. T., 2011, A&A, 532, A17

This paper has been typeset from a TEX/LATEX file prepared by the author.